Pergamon

Int. J. Solids Structures Vol. 33, No. 28, pp. 4143–4166, 1996

0020-7683/96 $15.00 + .00

0020-7683(95)00271-5

A MIXED MODE I/II INELASTIC LINE SPRING

BJØRN SKALLERUD
Division of Applied Mechanics, The Norwegian Institute of Technology, N-7034, Trondheim, Norway

(*Received* 6 *February* 1995; *in revised form* 23 *October* 1995)

Abstract—In many practical situations a cracked component may be subjected to mixed mode deformations. One important situation where this is relevant is surface cracked tubular joints applied in the offshore industry. Mixed mode affects both the deformation characteristics and fracture initiation capacity of the component, hence, an analysis model for numerical simulation should account for this. A finite element model consisting of solid elements is one approach to solve such problems. For complex components like a tubular joint, a very efficient model is obtained by means of shell finite elements. The cracked sections may be accounted for, utilizing line spring elements. Earlier work has concentrated on the Mode I deformation of the line spring. In the present study a mixed mode I/II elastic-plastic line spring is derived. The performance of the simple model is compared to continuum solutions obtained by means of detailed plane strain FE analyses. Both load vs deformation and J-integral performance of the line spring are considered in the comparisons.

INTRODUCTION

Nonlinear fracture mechanics has developed into an engineering tool due to the need for assessing defects in critical components loaded into the elastic-plastic regime. The methodology has been applied extensively in analysis of pressure vessels. For simple crack geometries and nonlinear elastic material behaviour (power hardening), there exist tabulated solutions of crack tip load parameters like the J-integral vs external loading (Rice, 1968a, Shih and Hutchinson, 1976, Goldman and Hutchinson, 1975, Shih *et al.*, 1981). This enables a rapid check of crack criticality, if $J_{applied} < J_{critical}$ a safe condition is confirmed.

Due to the geometric stress concentrations in tubular joints in offshore steel platforms, it is not seldom that surface cracks develop in the hot spots. The cracks are mainly caused by the fatigue damage accumulation process due to the cyclic environmental loads, and are typically located at the weld toe of the welds joining the chord and brace members. When the cracks are discovered by inspection, it is important to be able to predict possible further growth in order to decide convenient repair timing. First, a fatigue crack growth prediction is necessary. In this respect the linear elastic fracture mechanics concepts may be applied. Second, the behaviour of the crack during an overload (e.g., an extreme storm) has to be known in order to predict possible brittle/ductile fractures. If a brittle fracture of a heavily loaded joint should occur, insufficient structural safety against global collapse may be the result. Ductile fracture is more beneficial, as significant load carrying capability may still be maintained during a stable crack tearing process. Recently, the nonlinear fracture mechanics methodology has been investigated for capacity assessments of cracked tubular joints (Skallerud *et al.*, 1994, Skallerud, 1995, Cheaitani and Burdekin, 1994). Even for intact braces and chords the stress transmittal between them is complex, and introducing cracks in the brace/chord intersection further complicates this picture.

A large amount of research over the last years has been focused on triaxiality effects on the stress and strain fields in the crack region, and the corresponding effect on initiation and growth of the crack. Important results have emerged, e.g., lack of constraint in cracked regions in components loaded with predominant tension in the ligament, and variation of hydrostatic stress along the crack front of semi-elliptical surface cracks (McMeeking and Parks, 1979, Shih and German, 1982, Brocks *et al.*, 1988). These results have mainly been obtained for simple geometries like flat plates, with much simpler stress conditions than those in a tubular joint.

The most important feature of the J-integral is its ability to describe the magnitude of the crack tip stress and strain field (Hutchinson, 1968, Rice and Rosengren, 1968). The asymptotic analysis at the crack tip leads to the HRR-fields given by $\varepsilon_{ij} \propto (J/r)^{n/n+1} \cdot \varepsilon'_{ij}(\theta; n)$, $\sigma_{ij} \propto (J/r)^{1/n+1} \cdot \sigma'_{ij}(\theta; n)$, where r, θ are the polar coordinates relative to the undeformed crack tip; ε'_{ij} and σ'_{ij} are dimensionless functions, n is the hardening exponent in a power hardening material

$$\left(\varepsilon_{ij} = \tfrac{3}{2}\varepsilon_y \left(\frac{\sigma_{eq}}{\sigma_y}\right)^{n-1} \frac{\sigma_{ij} - 1/3\sigma_{kk}\delta_{ij}}{\sigma_y}\right).$$

Current research expands the theory to account for the first non-singular term in the power series solution (Betegon and Hancock, 1991, O'Dowd and Shih, 1992, Chao *et al.*, 1994). The above work has, however, concentrated on Mode I deformations of the crack, i.e., the opening mode. In many practical situations Mode II (sliding) and Mode III (tearing) also occur, and should be accounted for. Shih (1974) has extended the HRR solution to account for Mode I and II in small scale yielding. Skallerud (1995) points out the significant Mode II in surface cracked tubular joints. Cheaitani and Burdekin (1994) address the large Mode III when the crack becomes through thickness in such joints. As analyses of cracked tubular joints are essential regarding the assessment of the offshore platform safety, the problem of mixed mode has to be addressed.

The present investigation is directed towards the Mode I/II combination, and hence is relevant for surface cracked tubular joints. The motivation stems from the fact that mixed mode loading leads to mixed mode contributions in the J-integral. If one assumes self-similar crack growth for a cracked plate in plane stress, the material being perfectly plastic, the Dugdale model gives the connection between J and the crack tip opening displacement in Mode I and II:

$$\begin{aligned} J_{\mathrm{I},p} &= \sigma_y \delta_{\mathrm{I},cracktip} \\ J_{\mathrm{II},p} &= \tau_y \delta_{\mathrm{II},cracktip} \end{aligned} \tag{1}$$

In combined loading, and self-similar crack growth, the total J may be assumed to be $J_{\mathrm{I},p} + J_{\mathrm{II},p}$. Separation of J-type of parameters into Mode I and II by means of the corresponding deformations has been employed by Ishikawa *et al.* (1979) for elastic material, and by Aoki *et al.* (1990) for elastic-plastic material. In plane strain $J_{\mathrm{I},p}$ relates to the crack tip opening displacement by means of a constraint factor m that depends on crack geometry, loading, and hardening conditions in the ligament, i.e., $J_{\mathrm{I},p} = m\sigma_y \delta_{\mathrm{I},cracktip}$ (Shih, 1981).

For linear elastic materials the combined J is expressed via the stress intensity factors as

$$J_e = J_{\mathrm{I},e} + J_{\mathrm{II},e} = (K_{\mathrm{I}}^2 + K_{\mathrm{II}}^2)/E' \tag{2}$$

E' is Young's modulus in plane stress and $E/1-\nu^2$ in plane strain.

Kishimoto *et al.* (1980) have derived a general expression for J, denoted $\hat{J}$, that accounts for elastic-plastic material in the incremental sense and crack growth out of the plane given by the initial crack. Simplifying to isothermal conditions and small scale yielding, with vanishing body forces, the generalized relationship reads:

$$\begin{aligned} \hat{J}_k &= \int_\Gamma \left(W_e n_k - T_i \frac{\partial u_i}{\partial x_k}\right) \mathrm{d}\Gamma + \iint_A \sigma_{ij} \frac{\partial \varepsilon_{ij}^p}{\partial x_k} \mathrm{d}A, \quad (k = 1, 2) \\ \hat{J} &= \hat{J}_1 \cos\theta + \hat{J}_2 \sin\theta \end{aligned} \tag{3}$$

Γ is any counter clockwise path surrounding the crack tip, A is the area enclosed by Γ, and θ is the crack increment angle with respect to the original crack axis. W_e is the elastic strain

energy density. One notes that for elastic material and $\theta = 0$, $\hat{J} = J$. Furthermore, in mixed mode loading, contributions of Mode I and II will occur in both $\hat{J}_k$, cf. also eqns (1) and (2). Hence, irrespective of whether one assumes self-similar crack growth or not, the J or $\hat{J}$ employed in a fracture assessment contains mixed mode contributions.

In some commercial software codes calculation of J is implemented, and is determined by means of the virtual crack extension method combined with plane stress/strain elements or solid elements (Parks, 1974, Li *et al.*, 1985). With this, an account of mixed mode is obtained. For a three-dimensional surface crack in a complex component like a tubular joint the work in generating FE-meshes with solid elements is substantial. Usually, the number of elements through thickness in the brace/chord intersection region is kept low in order to have manageable problem sizes. This may introduce inaccuracies in the J-integral computation irrespective of the potential of computing accurate J-integrals for a finer mesh. A very convenient way of analyzing shell type of structures with surface flaws, and obtaining J-integrals, is the combination of shell and line spring finite elements (Rice and Levy, 1972, Parks, 1981, Parks and White, 1982). The reduction in the number of unknowns in the structural equation system given by the incremental principle of virtual work is large compared to a solid FE model. The effort in mesh generation is also reduced significantly. As the edge crack is the basic case for the line spring, computed values of a line spring based J for a surface crack will be more accurate in the center compared to positions approaching the surface at the crack ends. However, good accuracy of calculated J-values, both elastic and plastic, for semi-elliptical surface cracked shells have been obtained (Parks and White, 1982, White *et al.*, 1983, Shiratori and Miyoshi, 1983, Huang and Hancock, 1988). Although the J-values calculated by means of the line spring account for Modes I, II, III elastically, only Mode I is accounted for plastically. This model deficiency is addressed in the present study. An elastic-plastic line spring accounting for Mode I and II is derived, motivated by the efficient computer analysis obtained by such a method, and the need for accounting for mixed mode contributions in fracture assessments. First, the simple mixed mode inelastic line spring model is derived. Then some simulations are discussed, presenting quantitative and qualitative features of the model. The results are compared to continuum solutions of mixed mode loaded flat plates with cracks, analyzed by means of the program ABAQUS (Hibbitt *et al.*, 1992). Finally, some improvements of the model are pointed out.

LINE SPRING MODEL

Elastic stiffness

Figure 1 illustrates the main concepts of the line spring approach. Taking an intersection at some x-coordinate, the surface crack is simplified by an edge cracked strip with the same remaining ligament as for the surface crack at the same coordinate. The crack leads to additional deformations in the shell, denoted δ, θ, ξ for the axial, rotation, and shear deformation, respectively. The work conjugate forces are denoted N, M, V. Figure 1c shows the line spring for bending, continuously distributed along the x-axis, discretized to

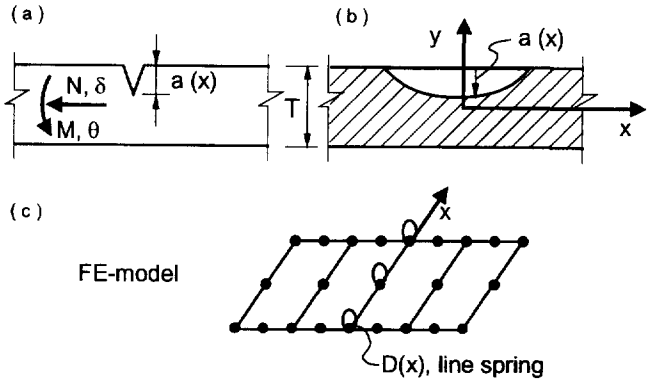

Fig. 1. Line spring concepts.

nodal values by, e.g., means of the principle of virtual work, hence compatible with the actual shell FE-formulation (8 nodes shown). Rice and Levy (1972) derived the elastic line spring for the extensional and rotational degrees of freedom. In the present study, shear deformations are also included. In order to obtain the elastic compliance of the cracked section, the concept of energy release rate is employed. In a load controlled situation the energy release rate is:

$$\mathcal{G} = \tfrac{1}{2} Q_i \frac{\partial q_i}{\partial a}, (i = 1, 2, 3)$$

$$\mathbf{Q} = [N, M, V]^{\mathrm{T}}, \mathbf{q} = [\delta, \theta, \xi]^{\mathrm{T}} \tag{4}$$

The elastic compliance of the cracked section connects the deformations and loads by:

$$\begin{aligned} \delta &= C_{NN} N + C_{NM} M \\ \theta &= C_{MN} N + C_{MM} M \\ \xi &= C_{VV} V \\ C_{NM} &= C_{MN} \end{aligned} \tag{5}$$

Here it is assumed no influence of shear deformations on extension and rotation, and vice versa. Now eqn (4) becomes:

$$\mathcal{G} = \frac{1}{2}\left(N^2 \frac{\partial C_{NN}}{\partial a} + 2NM \frac{\partial C_{NM}}{\partial a} + M^2 \frac{\partial C_{MM}}{\partial a} + V^2 \frac{\partial C_{VV}}{\partial a} \right) \tag{6}$$

Additionally, one has from fracture mechanics theory the connection between $\mathcal{G}$ and stress intensity factors. This leads to the elastic compliances in the following way:

$$K_{\mathrm{I},N} = \frac{N}{t}\sqrt{\pi a}(1.12 - 0.23\alpha + 10.6\alpha^2 - 21.7\alpha^3 + 30.4\alpha^4) = \sigma_N \sqrt{\pi a} \cdot f_N \tag{7}$$

$$K_{\mathrm{I},M} = \frac{M}{\frac{1}{6}t^2}\sqrt{\pi a}(1.12 - 1.39\alpha + 7.3\alpha^2 - 13\alpha^3 + 14\alpha^4) = \sigma_M \sqrt{\pi a} \cdot f_M$$

$$K_{\mathrm{II},V} = \frac{V}{t}\sqrt{\pi a} f_N = \tau_V \sqrt{\pi a} \cdot f_N$$

$$\alpha = a/t$$

$$\mathcal{G} = \frac{K_{\mathrm{I}}^2}{E'} + \frac{K_{\mathrm{II}}^2}{E'} = \frac{1}{E'}(\sigma_N^2 f_N^2 + 2\sigma_N \sigma_M f_N f_M + \sigma_M^2 f_M^2 + \tau_V^2 f_N^2)\pi a$$

$$\Rightarrow C_{NN} = \frac{2\pi}{E' t^2}\int_0^a a f_N^2 \, \mathrm{d}a \tag{8}$$

$$C_{MM} = \frac{2\pi}{E' \frac{1}{36} t^4}\int_0^a a f_M^2 \, \mathrm{d}a$$

$$C_{NM} = \frac{2\pi}{E' \frac{1}{6} t^3}\int_0^a a f_N f_M \, \mathrm{d}a$$

$$C_{VV} = \frac{2\pi}{E' t^2}\int_0^a a f_N^2 \, \mathrm{d}a$$

$$\mathbf{q} = \mathbf{C}_e \cdot \mathbf{Q}$$

The f_i ($i = N, M, V$) factors account for the effect of finite thickness on the crack tip stress field, and are determined by Gross and Srawley (1965) (note that $f_V = f_N$). Other factors exist, and may be applied in a similar way.

As most FE codes are based on a displacement formulation, the stiffness is used. This is obtained by inverting the compliance matrix:

$$\mathbf{Q} = \mathbf{D}_e \cdot \mathbf{q} = \mathbf{C}_e^{-1} \cdot \mathbf{q} \tag{9}$$

Plastic interaction surface

Rice (1972) has derived a yield surface for the ligament in Mode I loading (N, M), based on slip line theory for deep cracks, and a ligament loaded predominantly in tension, i.e., an upper bound solution:

$$f(N, M; \tau_y, c) = \left[\frac{\dfrac{N}{2\tau_y c} - 0.3}{0.7}\right]^2 + 9\left[\frac{M + N(t-c)0.5}{2\tau_y c^2}\right]^2 - 1 \tag{10}$$

Here τ_y is the shear yield stress, and c is the remaining ligament size. Lee and Parks (1993) have further computed Mode I yield surfaces for general load combinations (M, N) and crack depths. For mixed mode loading the slip line field is complicated, and an upper bound solution analogous to eqn (10) is not known to the author. In this study a lower bound solution is employed due to its simplicity. It follows the approach by Merkle and Corten (1974), but also includes shear force (Mode II). By assuming the outer parts of the ligament carries the bending moment, and central part carries axial and shear force, the lower bound yield surface reads

$$f(N, M, V, \sigma_y; c) = \left[\frac{N}{N_p}\right]^2 + \left[\frac{M + N(t-c)0.5}{M_p}\right] + \left[\frac{V}{V_p}\right]^2 - 1$$

$$N_p = \sigma_y c, \quad M_p = \tfrac{1}{4}\sigma_y c^2, \quad V_p = \frac{\sigma_y}{\sqrt{3}} c \tag{11}$$

Figure 2 depicts the yield surfaces given by eqns (10) and (11) in the first octant, with $V = 0$ for the latter. In Fig. 2a the uniaxial yield stress applied in the lower bound yield surface is multiplied by $2/\sqrt{3}$ in order to account for plane strain, whereas in Fig. 2b the yield stress is multiplied by $1.26*2/\sqrt{3}$ in order to account for the increased stress due to the crack (Green and Hundy, 1956). The factor 1.26 is derived for a ligament in dominating bending and for N approximately less than $0.5\sigma_y c$. In Fig. 2b the factor is utilised for ligaments with higher axial loads also. It is clear that plasticity will develop earlier for the lower bound solution, but the lower bound solution in Fig. 2b matches the upper bound curves quite well for $a/t > 0.25$. Effects of this are addressed subsequently. Equation (10) is not intended for use in dominating bending, hence is the comparison for this case not representative; e.g., in ABAQUS the surface is modified for such cases. Furthermore, the factor 1.26 is only valid for deep cracks, and should not be utilised for $a/t < 0.25$.

Elastic-plastic stiffness

The derivation of the elastic-plastic stiffness of the mixed mode line spring follows classical plasticity theory, i.e., assuming an additive decomposition of the elastic and plastic

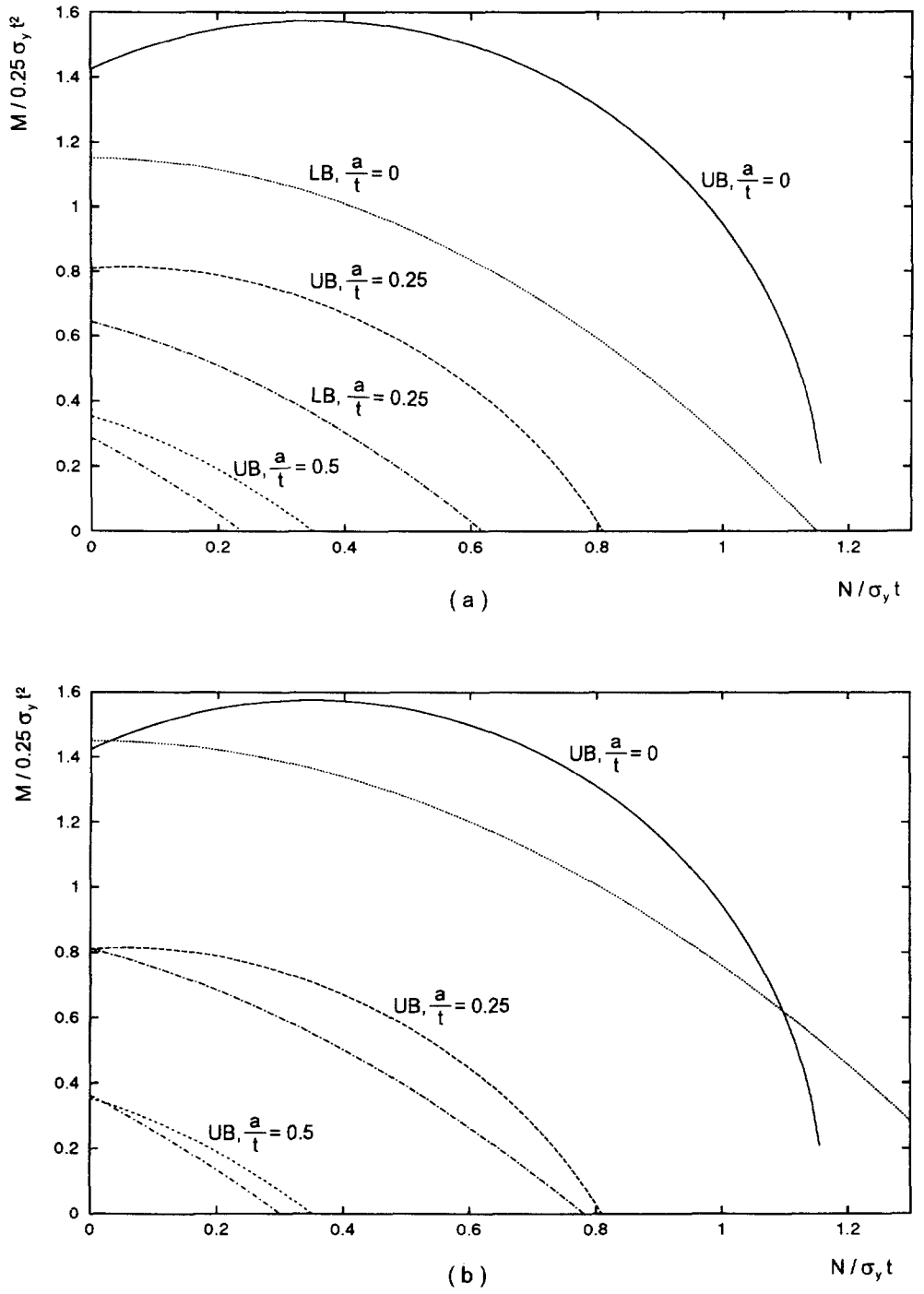

Fig. 2. Comparison of upper and lower bound yield surfaces (Mode I only).

line spring deformation increment, associated flow rule, plastic consistency, and an isotropic hardening rule:

$$\mathrm{d}\mathbf{q} = \mathrm{d}\mathbf{q}_e + \mathrm{d}\mathbf{q}_p$$

$$\mathrm{d}\mathbf{q}_p = \mathrm{d}q\frac{\partial f}{\partial \mathbf{Q}}$$

$$\mathrm{d}f = \frac{\partial f}{\partial \mathbf{Q}}\cdot \mathrm{d}\mathbf{Q} + \frac{\partial f}{\partial \sigma_y}\mathrm{d}\sigma_y = 0 \tag{12}$$

$$\Rightarrow \mathrm{d}\mathbf{Q} = \mathbf{D}_{ep} \cdot \mathrm{d}\mathbf{q} = \mathbf{D}_e \cdot \mathrm{d}\mathbf{q} - \mathrm{d}q\mathbf{D}_e \cdot \frac{\partial f}{\partial \mathbf{Q}} \tag{13}$$

The hardening rule is obtained by the argument that the plastic work increment of the stress resultants is equal to the continuum work increment integrated over the plastified ligament region:

$$\mathrm{d}W_p = \mathbf{Q} \cdot \mathrm{d}\mathbf{q}_p = \int_{A_{plastic}} \sigma_{eq}\, \mathrm{d}\varepsilon_{p,eq}\, \mathrm{d}A$$

$$\mathrm{d}\varepsilon_p = \frac{\mathrm{d}\sigma_y}{E_p} \tag{14}$$

Following Parks and White (1982), they argue that the continuum work is proportional to the averaged yield stress over the ligament multiplied by some plastically deforming area governed by ligament size, and they introduce a proportionality factor, denoted k herein:

$$\mathrm{d}W_p = \mathbf{Q} \cdot \mathrm{d}q \frac{\partial f}{\partial \mathbf{Q}} = k\sigma_y \frac{\mathrm{d}\sigma_y}{E_p} c^{n'} \tag{15}$$

Knowing the current plastic modulus E_p, $\mathrm{d}\sigma_y$ is expressed in terms of $\mathrm{d}q$, and is inserted in eqn (12). Solving for $\mathrm{d}q$ the elastic-plastic stiffness reads:

$$\mathrm{d}\mathbf{Q} = \left(\mathbf{D}_e - \frac{\left(\frac{\partial f^{\mathrm{T}}}{\partial \mathbf{Q}} \cdot \mathbf{D}_e\right)^{\mathrm{T}} \left(\frac{\partial f^{\mathrm{T}}}{\partial \mathbf{Q}} \cdot \mathbf{D}_e\right)}{\frac{\partial f^{\mathrm{T}}}{\partial \mathbf{Q}} \cdot \mathbf{D}_e \cdot \frac{\partial f}{\partial \mathbf{Q}} - \frac{\partial f^{\mathrm{T}}}{\partial \mathbf{Q}} \cdot \mathbf{Q} \frac{\partial f}{\partial \sigma_y} \frac{E_p}{\sigma_y k c^{n'}}} \right) \cdot \mathrm{d}\mathbf{q} \tag{16}$$

From the slip line field solution Parks and White argue that the exponent n' is 2 and the k-factor of order unity. The value of k is investigated subsequently, combined with $n' = 2$. Equation (16) is on a form that readily is implemented in a FE-shell code based on displacement formulation. Note that although $\mathbf{D}_e$ has no interrelation between Mode I (N, M) and Mode II (V), $\mathbf{D}_{ep}$ does.

J-integral calculation

The elastic part of the mixed mode J may be determined directly from the current load level:

$$J_e = \frac{K_{\mathrm{I}}^2}{E'} + \frac{K_{\mathrm{II}}^2}{E'} \tag{17}$$

The plastic part is more difficult to obtain. As mentioned in the Introduction the Mode I plastic J may be derived from the crack tip opening displacement, provided a correction due to constraint, ligament load characteristics, and hardening is taken into account. In incremental form this reads:

$$\mathrm{d}J_{\mathrm{I},p} = m\sigma_y\, \mathrm{d}\delta_{\mathrm{I},cracktip,p} \tag{18}$$

It is known from analytical studies (Rice, 1975) that m is close to unity for ligaments predominantly loaded in tension, whereas for predominant bending of the ligament m approximately equals 2. Parks and White (1982) utilize the fact that the load vector should lie on the yield surface during crack growth

$$\left(\left.\frac{\mathrm{d}f}{\mathrm{d}c}\right|_{q_i} = 0\right)$$

and a constant ratio of plastic deformations during crack growth

$$\left(\text{i.e.}\left.\frac{(\partial\, \mathrm{d}\delta_p/\mathrm{d}\theta_p)}{\partial c}\right|_{\mathrm{d}\delta_p,\mathrm{d}\theta_p} = 0\right).$$

This leads to two equations with two unknowns,

$$\frac{\partial N}{\partial c}$$

and

$$\frac{\partial M}{\partial c},$$

that are used in the calculation of the plastic part of J. The following relationship for J_p holds in perfect plasticity (Rice, 1968b):

$$J_p = -\int_0^{q_{p,i}} \left.\frac{\partial Q_i}{\partial a}\right|_{q_{p,i}} \cdot \mathrm{d}q_{p,i} = \int_0^{q_{p,i}} \left.\frac{\partial Q_i}{\partial c}\right|_{q_{p,i}} \cdot \mathrm{d}q_{p,i} \Rightarrow \mathrm{d}J_{1,p} = \frac{\partial Q_i}{\partial c}\,\mathrm{d}q\,\frac{\partial f}{\partial Q_i} = m\sigma_y\,\mathrm{d}\delta_{1,cracktip,p} \tag{19}$$

The plastic crack tip opening displacement may be obtained from the slip line solution combined with the plastic extension and rotation increment of the ligament (Parks and White, 1982):

$$\mathrm{d}\delta_{1,cracktip,p} = \mathrm{d}\delta_p + \left(\frac{t}{2} - a\right)\mathrm{d}\theta_p \tag{20}$$

Hence, combining eqns (19) and (20), an m that varied between 1 and 2 was obtained. Lee and Parks (1993) have checked the validity of eqn (20), and found that for shallow cracks ($a/t < 0.3$) it overpredicts the crack tip opening displacement. Applying this method in order to determine m in combination with the lower bound yield surface does not lead to m varying in this range. A simple interpolation based on numerical testing is chosen here for m, simply:

$$m = 1 + (M'/M_p)^3 \tag{21}$$

M' is the sum of bending and the moment due to the axial load eccentricity. In pure ligament tension $m = 1$, and for increasing ligament bending m approaches 2. Shih (1981) has investigated the values of m for different hardening in HRR fields and large scale yielding (where component geometry may become influential). It is shown that for ligaments in predominant bending the large scale yielding value of m approximately equals the HRR value, i.e. ≈ 2, for low hardening materials ($n > 8$). Furthermore, for increasing axial load in the ligament m approaches 1 for low hardening materials. In order to assess eqn (21), the estimation relationships determined by Shih and Needleman (1984) are utilised. Assuming that $J = m\sigma_y\delta_{tip}$ and $\delta_{tip} = \delta + (t/2 - a)\theta$ for a deformation plastic material, employing the relationships for J, δ, θ from Shih and Needleman (1984) for an axially loaded plate in plane strain, the following results represent m in terms of axial displacement for $n = 10$: $1.44\delta^{0.1}, 2.22\delta^{0.1}, 2.46\delta^{0.1}$, for $a/t = 0.25, 0.5, 0.75$, respectively. As seen from

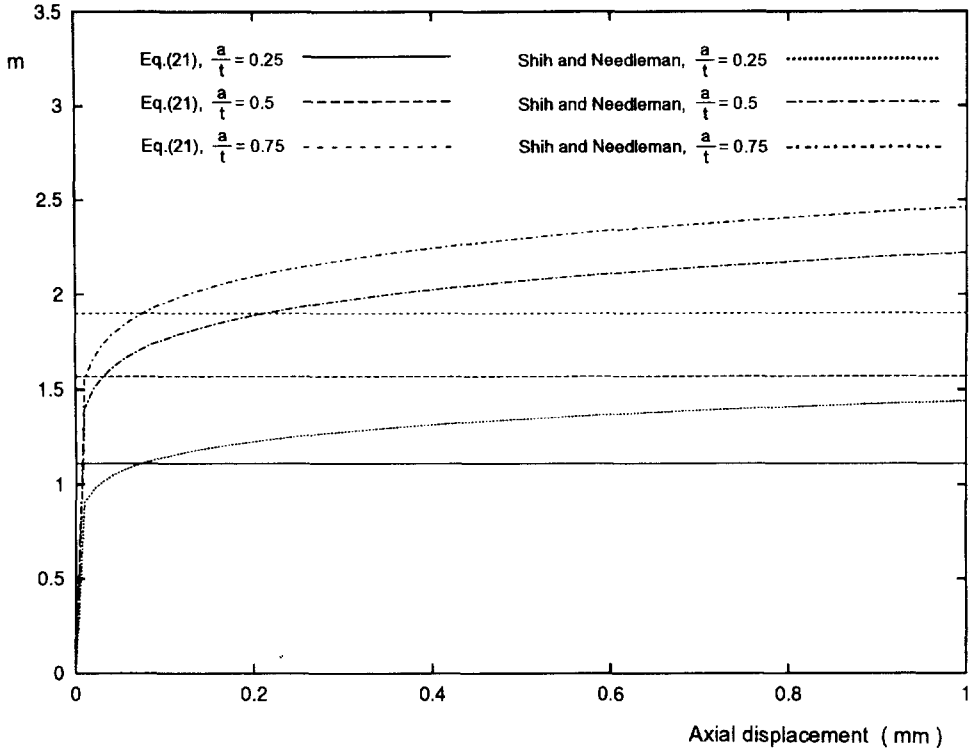

Fig. 3. Comparison of constraint factor m determined by eqn (21) and estimation procedures.

Fig. 3 the constraint depends on load level and degree of ligament bending, but eqn (21) approximates m reasonably for moderate plasticity. However, tabulated results as derived by Shih and Needleman (1984) may be utilised in improving the constraint calculation.

Extending to Mode II also, one could envisage a constraint factor m_{II}. Without detailed knowledge for this variable, the Mode I constraint factor is assumed for Mode II in this investigation. Hence, the total plastic J-increment is calculated from:

$$dJ_p = dJ_{I,p} + dJ_{II,p} = m\sigma_y\left[d\delta_p + \left(\frac{t}{2} - a\right)d\theta_p\right] + m\frac{\sigma_y}{\sqrt{3}}d\xi_p \tag{22}$$

By updating the deformation increment and yield stress due to hardening, the total J is determined, containing both elastic and plastic Mode I and II contributions. Note that, although the ligament deformation pattern due to the lower bound yield surface differs from the slip line deformation pattern, the *connection* between crack tip opening displacement and ligament deformations from the slip line field is employed as representative in calculating the Mode I plastic J in the present study. Furthermore, the interaction between normal stress and shear stress on plastic deformation in the ligament is neglected in eqn (22). For example for the von Mises yield surface in plane stress, the maximum overprediction in yield axial and shear stress is approximately 30%.

RESULTS

Calibration in Mode I, comparison with estimation procedures

First, the line spring model is investigated for Mode I only. The tabulated solutions for plane strain edge cracked strips loaded in tension and bending determined by Shih and Needleman (1984) are used as estimates for accurate fully plastic solutions. Hence, the quantitative performance of the line spring in large scale yielding is assessed. As modern structural steels usually are very ductile, fully plastic ligaments develop before fracture initiation. Therefore, the behavior of the line spring model should be representative for the

actual behaviour in this regime. Three different crack depths and two hardening levels are investigated ($a/t = 0.25, 0.5, 0.75$, and $n = 5, 10$). The two stress-strain curves are fit by four-linear curves, then the multilinear fits are applied in the line spring analyses.

Figure 4a shows the axial load vs axial displacement (normalised by $\sigma_y t$ and $\sigma_y t/E$, respectively) for the low hardening material and $a/t = 0.5$. The line spring is elastic-plastic, therefore the initial stiffness in the estimation procedure and the line spring differs (as it should). Approaching fully plastic conditions the line spring model with $k = 0.2$ and a yield surface σ_y multiplied with $1.26*2/\sqrt{3}$ matches the analytical result excellently. If σ_y only is corrected for plane strain ($2/\sqrt{3}$), use of the lower value $k = 0.02$ is better than $k = 0.2$. Figures 4b and c illustrate J vs axial load and axial displacement, respectively (J normalised by $\sigma_y^2 t/E$). One observes that utilising $k = 0.2$ and $\sigma_y := 1.26*2/\sqrt{3}\sigma_y$ in the yield surface gives a good approximation for the estimation curves, whereas for $k = 0.02$ and $\sigma_y := 2/\sqrt{3}\sigma_y$, J vs N is overpredicted and the accuracy of the line spring J vs axial displacement is acceptable. The deviation between the analytical results and the line spring results in the elastic-plastic transition may be reduced by improving the fit of the stress-strain curve applied in the line spring analyses to the power hardening material model employed in the analytical model

In Fig. 5 results for a highly hardening material are plotted. For the axial load vs axial displacement behaviour it is observed that correcting the yield stress in the lower bound yield surface with $1.26*2/\sqrt{3}$ combined with $k = 0.2$ corresponds reasonably to the analytical result, except for the elastic-plastic transition region, where an improved stress-strain curve fit would remedy the inaccuracy. Furthermore, if the yield stress only is multiplied with $2/\sqrt{3}$, $k = 0.02$ gives a too stiff line spring, and $k = 0.2$ gives a too flexible spring. hence, a k-value between 0.02 and 0.2 will give a reasonable line spring response prediction. Figure 5b accentuates that the line spring stress-strain curve should be fitted more accurately as the graph presents J values in the elastic-plastic transition region. The model parameter pair ($k = 0.2$, $1.26*2/\sqrt{3}\sigma_y$) gives, however, acceptable results in the fully plastic regime. For the J vs axial displacement plots in Fig. 5c, the corresponding line spring results slightly underpredict the estimation result (and will improve for a better stress-strain curve fit), whereas ($k = 0.2, 2/\sqrt{3}\sigma_y$) gives a good correspondence to the estimation curve.

Figure 6 shows the performance of the line spring for a deep crack and a low hardening material. Again, correcting the lower bound yield surface yield stress with $1.26*2/\sqrt{3}$ combined with $k = 0.2$ gives good correspondence to the analytical results, although there is conservative J vs displacement behaviour.

For the case $a/t = 0.25$ applying the factor 1.26 in correcting the yield surface yield stress is not acceptable, as the crack is too shallow. Hence, the line spring results in Fig. 7 contain only the correction $2/\sqrt{3}$ in the yield surface yield stress. For $k = 0.2$ the axial load versus axial displacement behaviour is acceptable, $k = 0.02$ leads to too stiff response. A k-value of 0.1 will improve the result. The overprediction in J vs axial load in Fig. 7b is significant for $k = 0.2$, where for J vs displacement a good correspondence is obtained. For the low hardening material results plotted in Fig. 8, $k = 0.02$ gives a good stiffness representation. However, the J integral is overestimated by the line spring method.

From the above Mode I investigation it may be concluded that for $a/t > 0.25$, combining $k = 0.2$ with $1.26*2/\sqrt{3}\sigma_y$ as yield stress in the yield surface gives acceptable correspondence to the estimation solutions derived by Shih and Needleman (1984). The line spring results may further be improved by refining the stress-strain curve employed (four linear segments). For $a/t = 0.25$ the yield stress was only multiplied with $2/\sqrt{3}$. $k = 0.2$ and 0.02 gave reasonable results regarding load vs deformation for the high and low hardening material, respectively. For such shallow cracks, however, an improved J calculation would require a more accurate relationship between the ligament deformations and the crack opening displacement than that given by eqn (20) (Lee and Parks, 1993).

Effect of Mode II

Figure 9 shows the effect of different levels of shear loading, leading to Mode II deformation, on the calculated response. The shear is applied proportionally to the axial force, $V = rv \cdot N$. The material is low hardening ($n = 10$), and $a/t = 0.5$. One sees that in

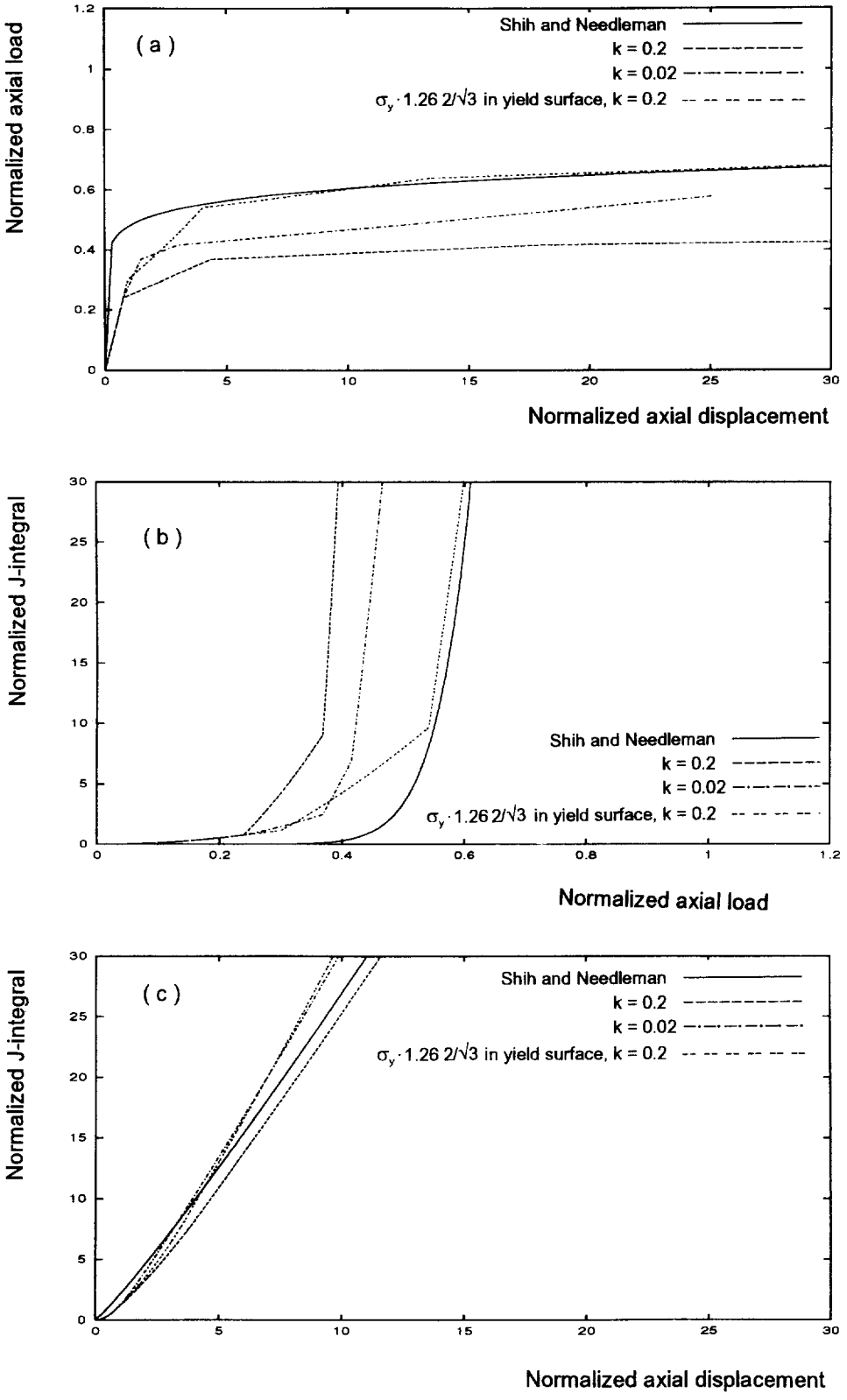

Fig. 4. Calibration of line spring model (Mode I), $a/t = 0.5$, $n = 10$.

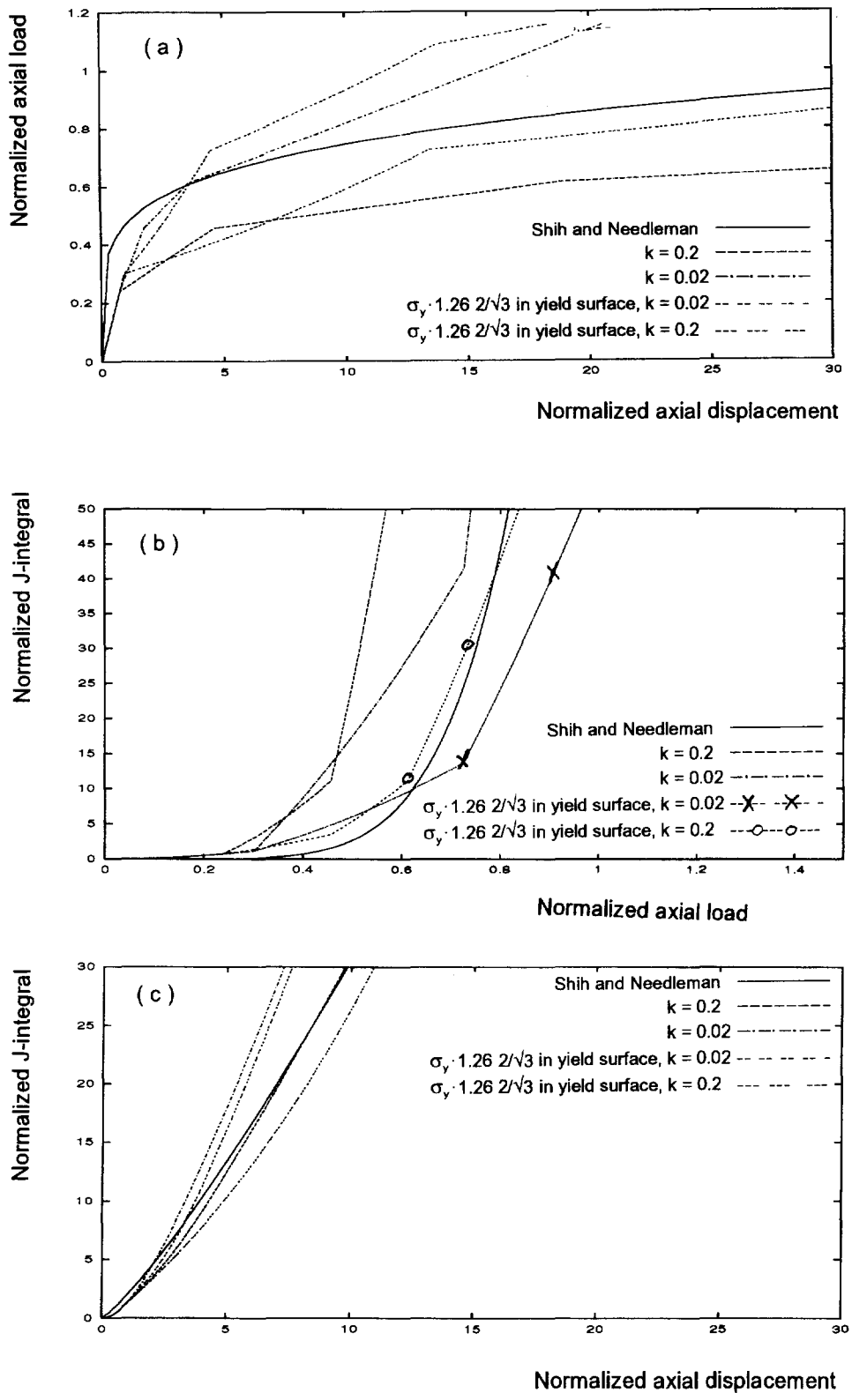

Fig. 5. Calibration of line spring model (Mode I), $a/t = 0.5$, $n = 5$.

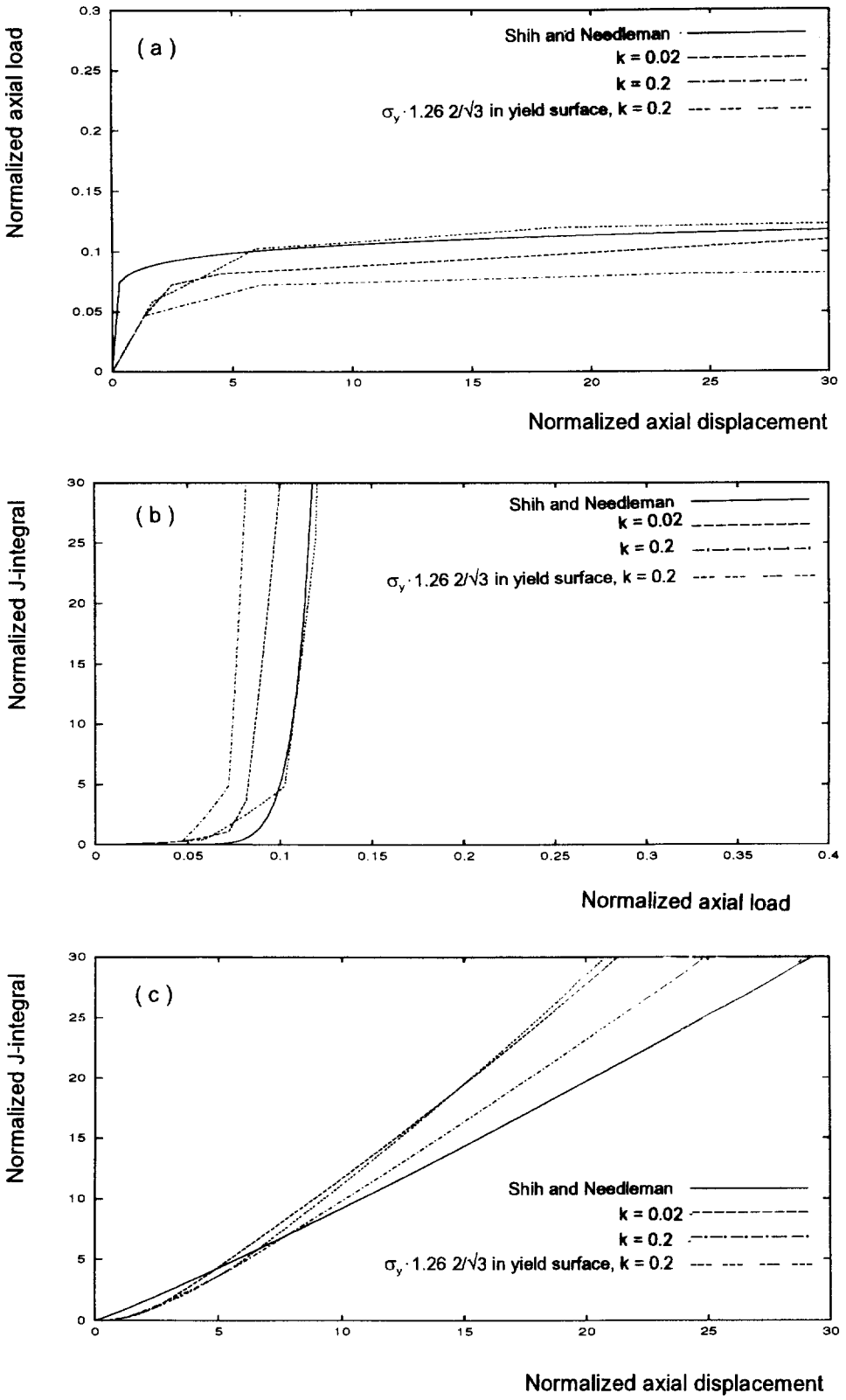

Fig. 6. Calibration of line spring model (Mode I), $a/t = 0.75$, $n = 10$.

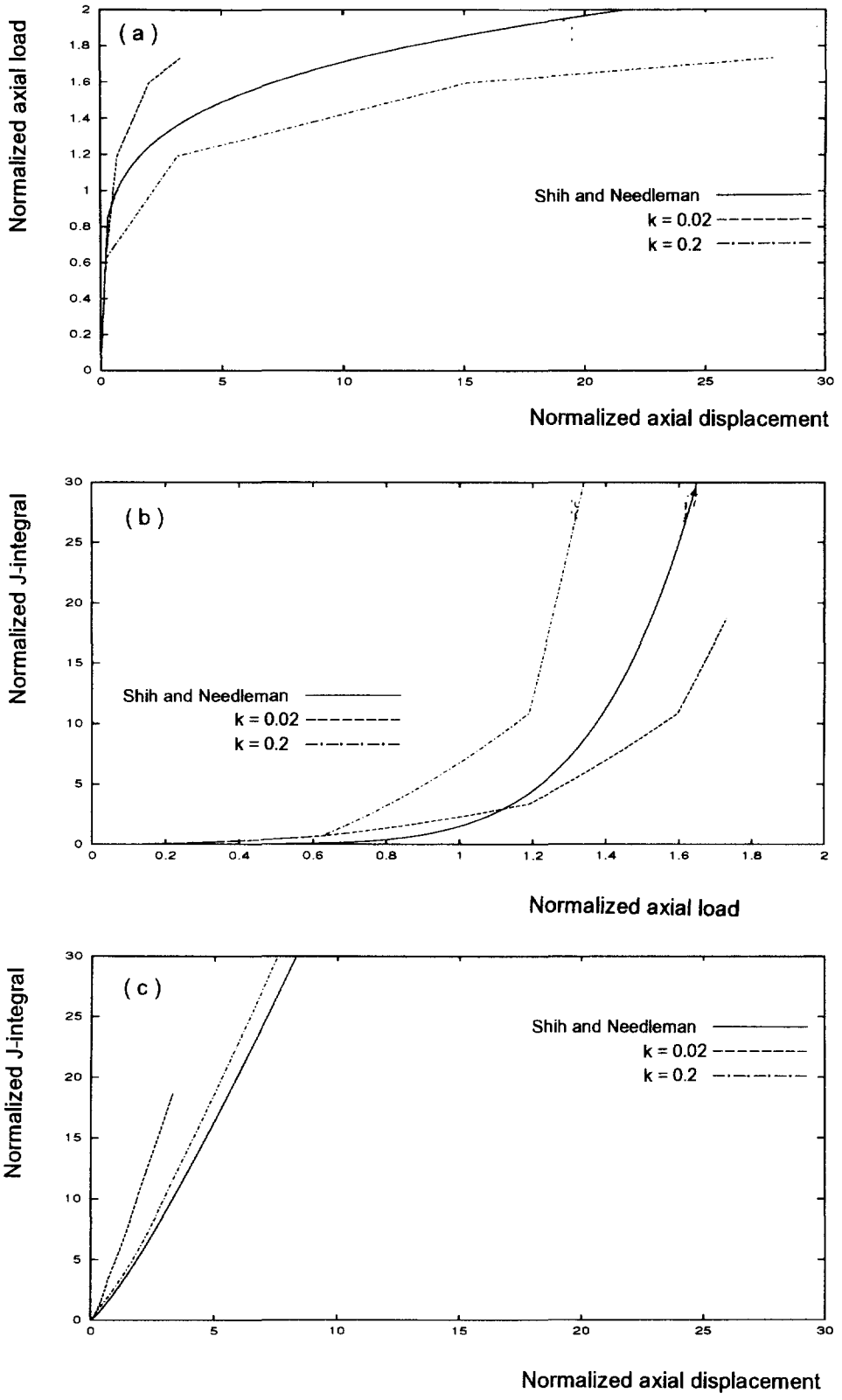

Fig. 7. Calibration of line spring model (Mode I), $a/t = 0.25$, $n = 5$.

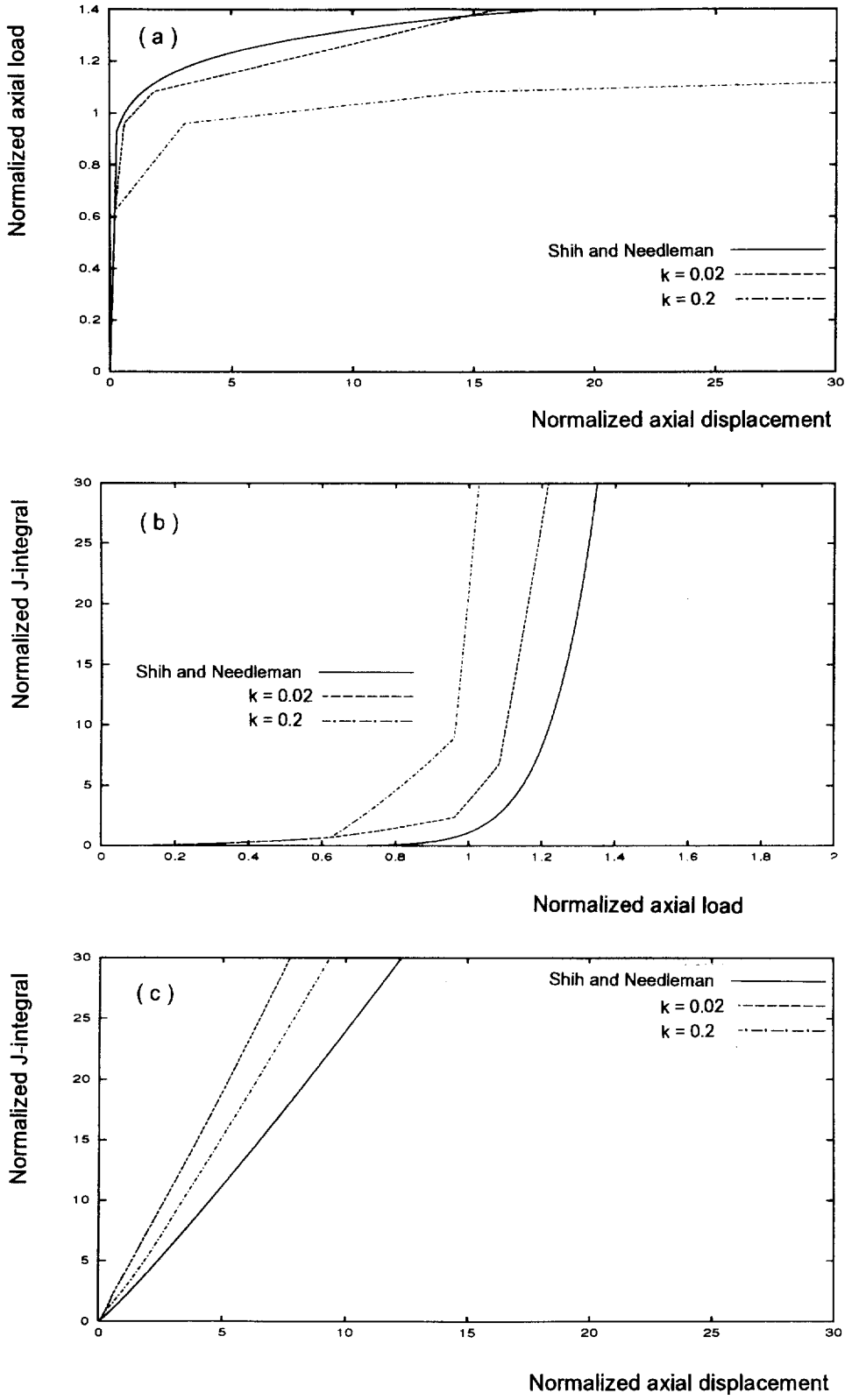

Fig. 8. Calibration of line spring model (Mode I), $a/t = 0.25$, $n = 10$.

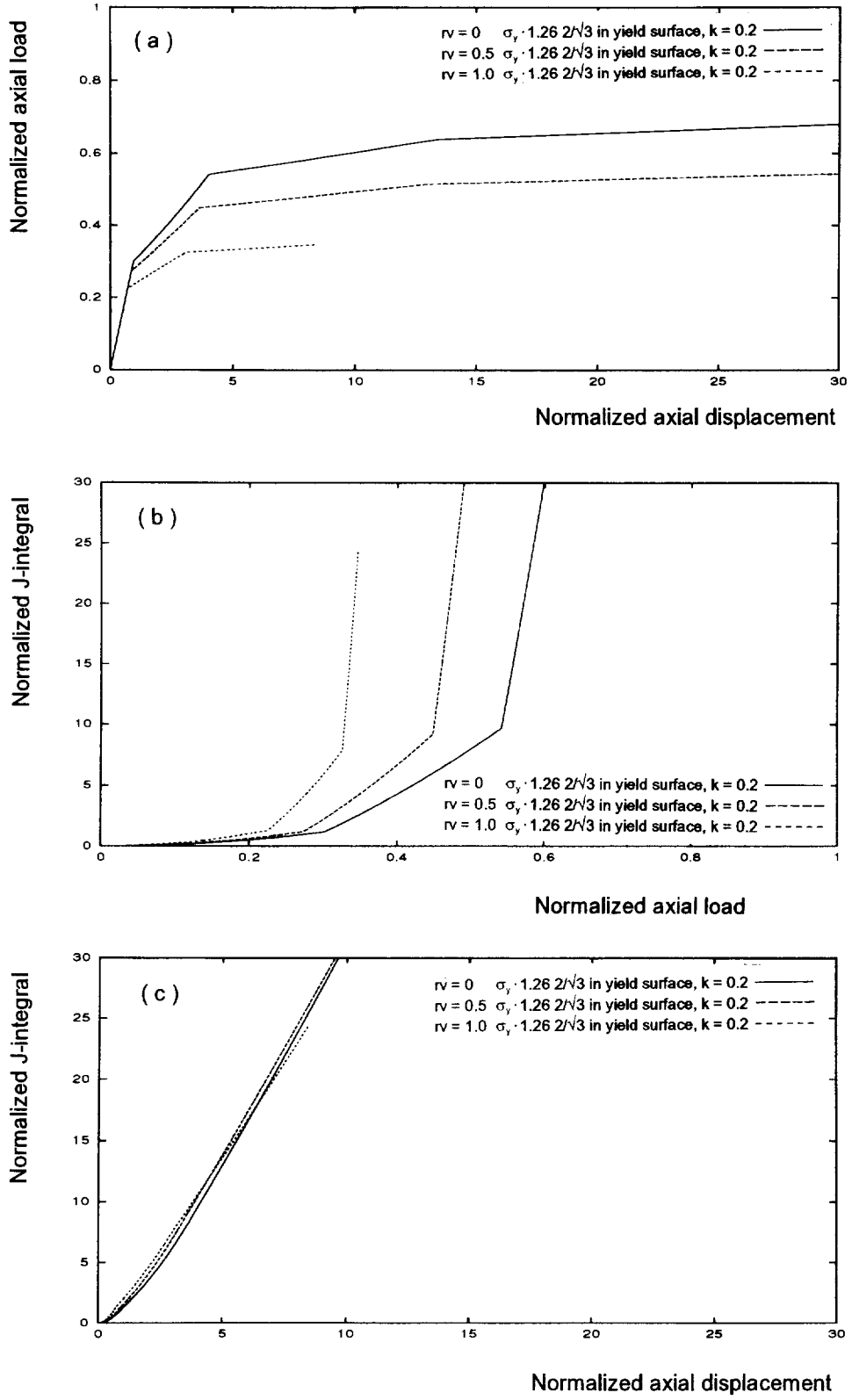

Fig. 9. Effect of shear force (Mode II), $a/t = 0.5$, $n = 10$.

load control, increasing the shear load has a substantial effect on the N–δ and J–N behaviour. However, from Fig. 9c an interesting result emerges (similar results apply for $a/t = 0.25$ and 0.75 also). It is observed that increasing the shear in a displacement controlled situation does not lead to a significant increase in total J. This indicates that in displacement controlled components, simpler line spring models may be employed. Considering eqn (11) the interaction between the bending moment and shear is between linear and quadratic, whereas for high axial load (small a/t) and shear force, the interaction is quadratic. The reason for the insensitivity in J to Mode II may be explained to a large extent by considering a ligament loaded in pure normal force and shear. Assume a linear plastic interaction between N and V for simplicity, and perfectly plastic material.

$$f = \frac{N'_p}{N_p} + \frac{V'_p}{V_p} - 1 = 0$$

$$V = rv \cdot N \Rightarrow N'_p = \sigma_y c/(1 + rv\sqrt{3}),\ V'_p = rv \cdot N'_p$$

Using an associated flow rule, one obtains the relation between plastic extension and shear deformation:

$$\delta_p = \lambda \frac{\partial f}{\partial N} = \lambda / N_p$$

$$\xi_p = \lambda \frac{\partial f}{\partial V} = \lambda / V_p$$

$$\Rightarrow \xi_p = \sqrt{3}\delta_p$$

For a perfectly plastic material in displacement control, with self-similar crack growth, J is given by:

$$J_p = J_{\mathrm{I},p} + J_{\mathrm{II},p} = \frac{\partial W_{\mathrm{I},p}}{\partial c} + \frac{\partial W_{\mathrm{II},p}}{\partial c}$$

$$= \sigma_y \delta_p \left(\frac{1}{1 + rv\sqrt{3}} + \frac{rv\sqrt{3}}{1 + rv\sqrt{3}} \right) = \sigma_y \delta_p \equiv J_{\mathrm{I},p}|_{V=0}$$

Hence, for a hardening material and a slightly more complicated yield surface (eqn (11)), the resulting J vs δ shows a similar behaviour (Fig. 9c).

Comparison with FE results in Mode I

As there exist no tabulated results for edge cracked strips in combined Mode I and Mode II loading, a FE study was carried out in order to have detailed solutions of such loading modes for comparison with line spring results. First, the case analysed is the same as that employed by Parks and White (1982): a tension loaded edge cracked strip in plane strain with $a/t = 0.5$. Hence, the only bending moment in the ligament is due to the eccentricity of N. The material model used for stress-strain behaviour in all simulations is a trilinear one, with initial yield stress of 490 MPa, linear slope for $\sigma < 700$ MPa and $\varepsilon_p < 0.1$, followed by non-hardening behaviour. This material corresponds to a low hardening material ($n \approx 20$). As the line spring model investigated herein is load driven, a small plastic modulus of 0.01 of the initial plastic modulus is employed for plastic strains above 0.1.

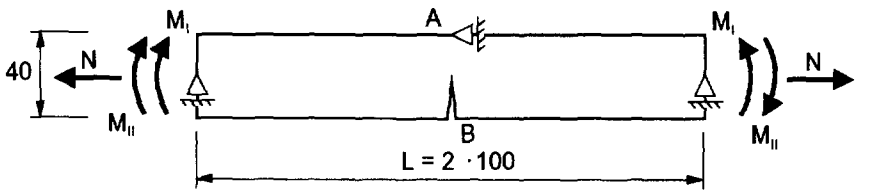

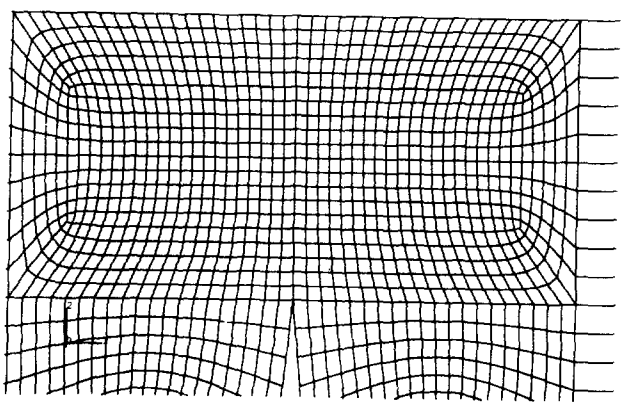

Fig. 10. Model for FE analyses.

Figure 10 illustrates the static model for the continuum solution, employed in the ABAQUS analyses (Hibbitt *et al.*, 1992), using isoparametric 8-noded, plane strain finite elements and the same material model for stress-strain as for the line spring. Note that the bending moment M_{II} leads to pure Mode II deformation of the crack. The stress resultants were applied by means of 17 nodal forces at each end. The element size in the ligament region is 0.025 times the thickness. The FE model consisted of 1732 elements and about 10,000 degrees of freedom. Default convergence criteria were employed in the analyses, e.g., for nodal forces the error was less than 0.005 at all nodes at convergent solution. A part of the ligament region, denoted intense deformation zone by Shih and Needleman (1984), consisted of approximately 20*40 elements, capturing the extension of the intense strain fields approaching the slip line solution at the highest load levels. As pointed out by Shih and Needleman (1984), if a deformation plastic material model is applied, then path dependencies in the J-integral reflect inadequacies in the FE-meshes. This was checked in the present study by first running some FE analyses with such a material model, resembling the trilinear stress-strain curve. In all analyses 9 contours were utilized in the J-computations. First, a reduced integration (2X2 Gauss points) element was investigated, i.e. the mesh in Fig. 10. The mesh in the ligament region consisted of rectangular elements with aspect ratio close to one, and no collapsed nodes at the crack tip. The J-value for the first ring of elements was disregarded. For the next eight rings the path dependency was less than 0.01 at all load levels compared to the average value. The elastic value differed by 0.7 percent for $a/t = 0.5$ compared to Tada *et al.* (1972), whereas for $a/t = 0.25$ the difference was even less. Additionally, the effect of using a focused mesh was investigated (this model consisted of fewer elements than in the rectangular FE-mesh). For contained plasticity, the difference in J for the two meshes was negligible. For load levels approaching limit load, the rectangular FE-mesh yielded J-values approximately 20% lower than those for the

focused mesh. The effect of interpolating the hydrostatic stress for nearly incompressible material by means of a hybrid 8-noded element was negligible compared to applying the reduced integration element. For these reasons the rectangular mesh of elements with reduced integration was employed in the continuum model, as variations of magnitude 10% result both from different numerical integration schemes (Dodds, 1985) and experimental scatter in critical J-values.

The axial displacement caused by the crack was obtained by subtracting $\delta_{nocrack} = NL/E't$ from the total displacement. Note that this correction presumes dominating elastic behaviour of the material outside the ligament region.

Figure 11a shows the axial force vs axial displacement (normalized by $\sigma_y t$ and $\sigma_y t/E$, respectively) for different values of the k-factor and yield stress, see eqn (15). The combination of $(k = 0.2, 1.26*2/\sqrt{3}\sigma_y)$ corresponds well to the FE result, both for axial load vs axial displacement, J vs axial load, and J vs axial displacement. The combination $(k = 0.02, 2/\sqrt{3}\sigma_y)$ results in a too flexible line spring, and overpredicts J in terms of axial load, but predicts acceptable values of J in terms of axial displacement. Note that the elastic stiffness is well represented by the line spring for this elastic-plastic material (this stiffness could not be assessed in the comparison to fully plastic estimations given above). The recent investigation by Lee and Parks (1995) shows that accounting for the fact that the crack size appears larger than the physical one due to the crack tip plastic zone, a very accurate elastic-plastic transition is obtained by the line spring. This effect is not considered herein.

Comparison with FE behaviour in pure shear (Mode II)

The case of pure Mode II was also analyzed. Figure 12a shows the shear force vs shear deformation for $a/t = 0.5$. The FE shear deformation is taken as the difference in vertical displacement between points A and B in Fig. 10. One observes that the line spring is too stiff in the elastic-plastic transition for $(k = 0.2, 1.26*2/\sqrt{3}\sigma_y)$, but for increasing plasticity the correspondence is excellent. It is well known that a Mode II crack tip plastic zone is larger than a Mode I plastic zone at the same load level. Hence, applying a crack size that accounts for the plastic zone would probably improve the elastic-plastic transition. The combination $(k = 0.02, 2/\sqrt{3}\sigma_y)$ is too flexible, but not unacceptable. Figure 12b shows the J-V behaviour for the line spring and continuum model. The correspondence is good when the effect of the crack on the stresses is accounted for (i.e., also employing the factor 1.26), considering the simple way of accounting for shear in the line spring. Not accounting for the stress elevation factor 1.26 leads to very conservative J line spring values. The J-ξ results are in excellent agreement with the continuum solution, Fig. 12c. This indicates that applying the same constraint factor in Mode I and Mode II for this crack and material is reasonable.

Comparison and FE results in combined axial force, bending moment, and shear (Mode I and II)

Figure 13 shows the case of $a/t = 0.5$, with a shear force 10% of axial load, and a factor 10 between bending moment and axial force, applied proportionally. Similar effects as presented in earlier graphs are observed: softer N-δ behaviour, overprediction in J-N, and reasonable agreement in the J-δ plots.

CONCLUDING REMARKS

Regarding efficiency, the advantages in a line spring based approach compared to solid element analyses of cracked shell structures are obvious. However, several simplifications are inherent in the model. Two main modelling aspects are important. First, in order to represent the increased flexibility of the cracked shell, the shell stress resultants (N, M, V) vs energy conjugate deformations in the line spring should be simulated with reasonable accuracy. The lower bound yield surface utilized in the present study leads to softer behaviour of the line spring in the plastic range compared to detailed plane strain FE analyses, but the deviation is not unacceptable. When the yield stress used in the yield surface accounts for the stress elevation due to the crack, i.e. multiplied by 1.26, the line

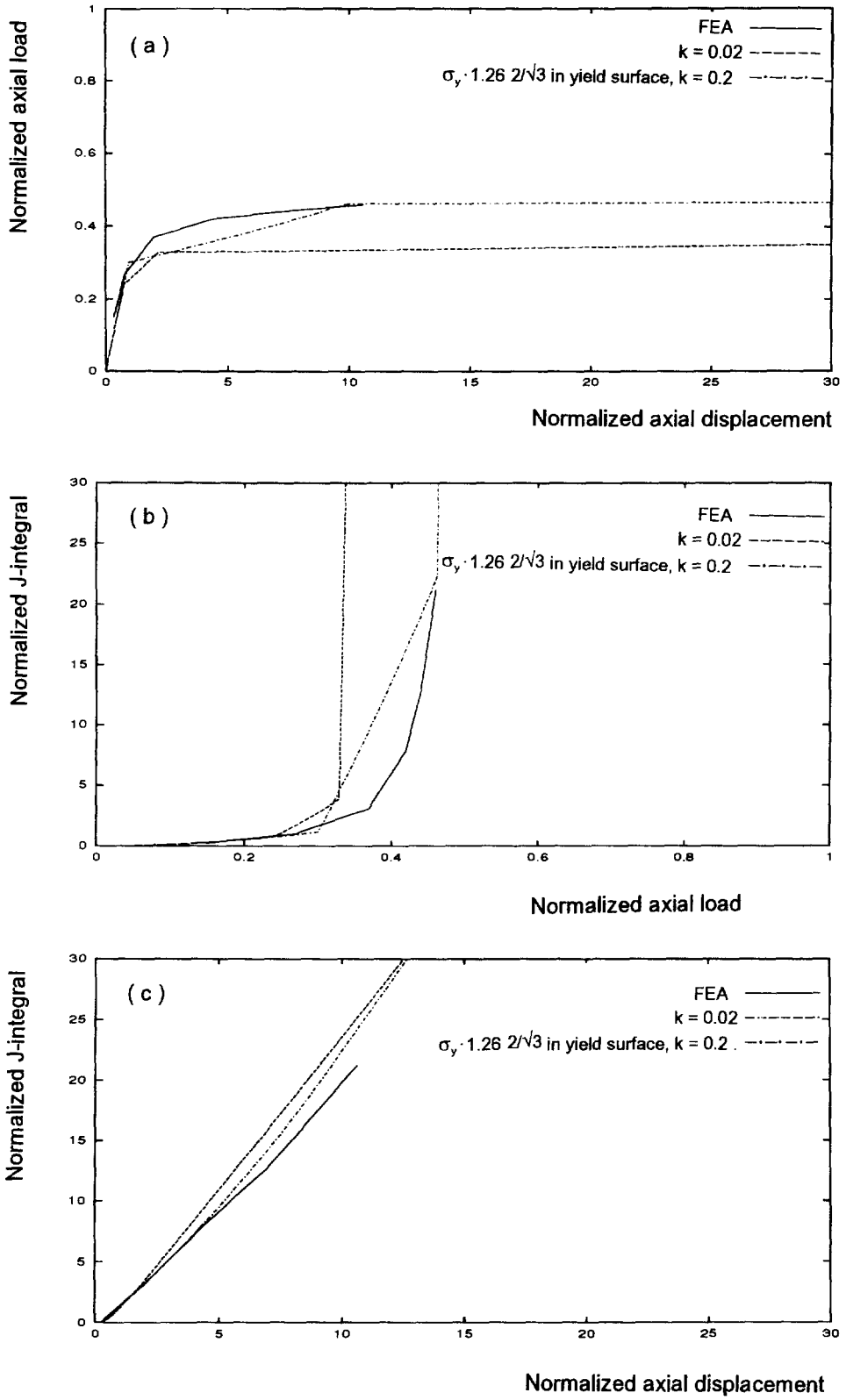

Fig. 11. Calibration of line spring model (Mode I), $a/t = 0.5$, $n \approx 20$.

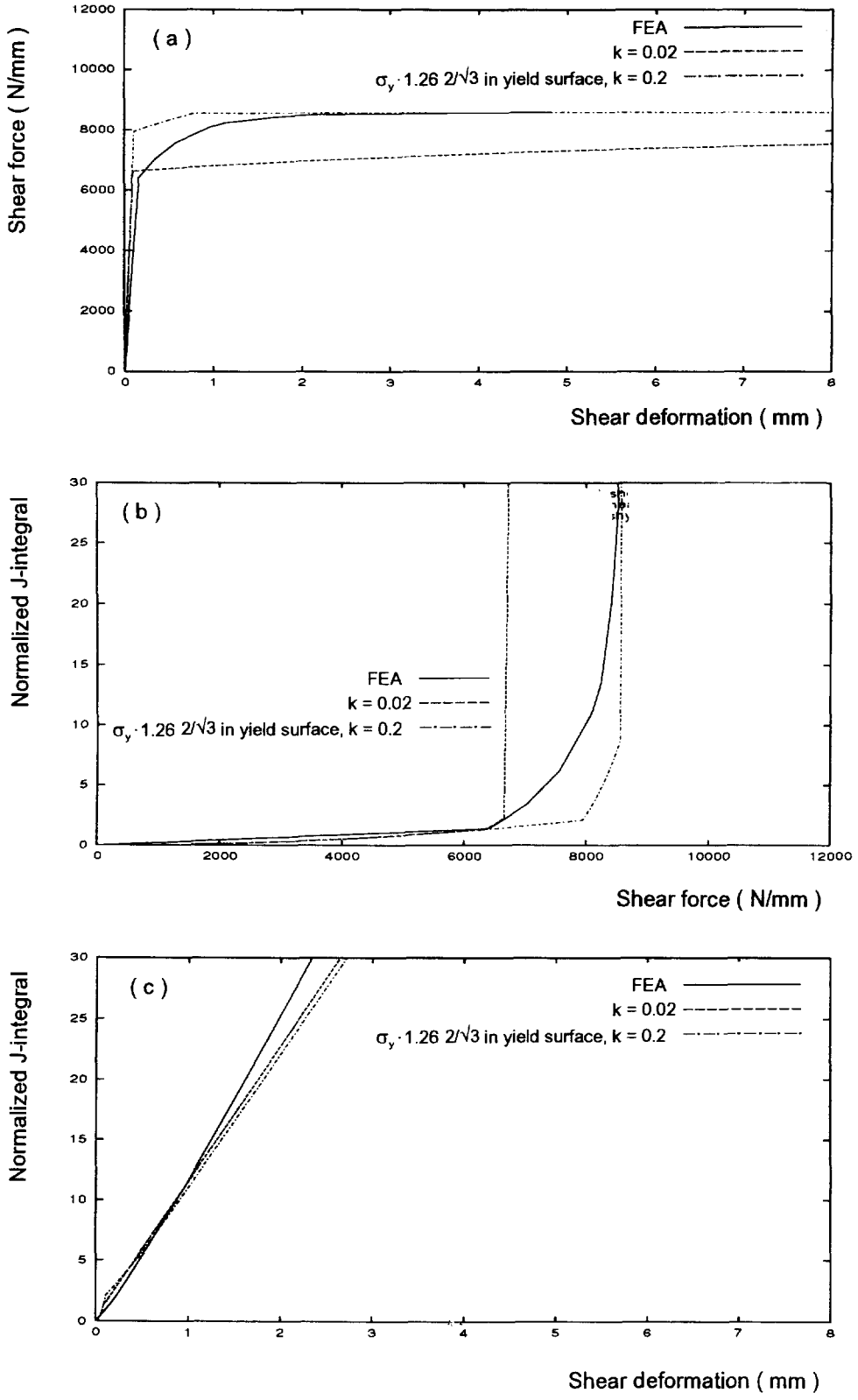

Fig. 12. Results in pure Mode II, $a/t = 0.5$.

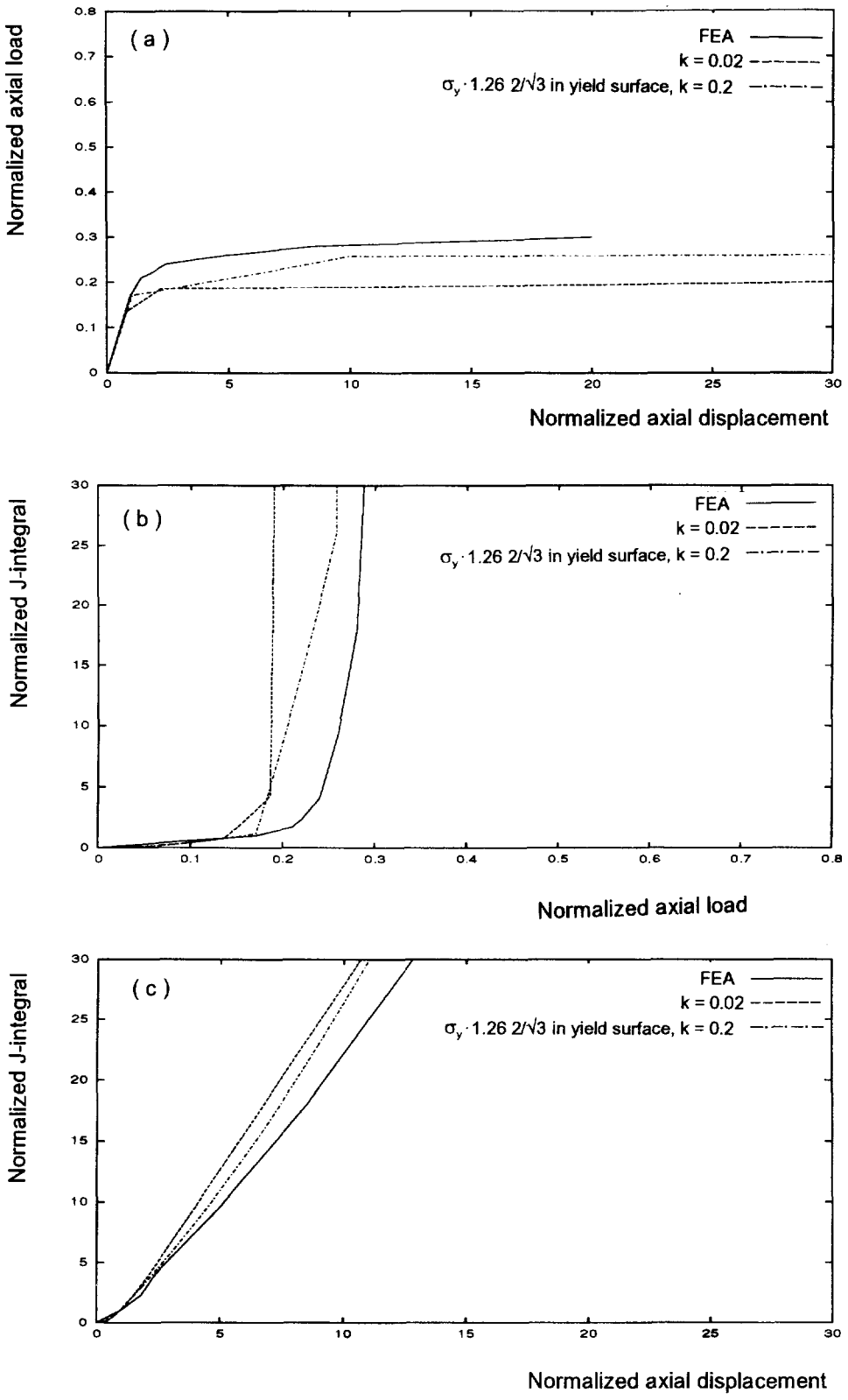

Fig. 13. Combined N, M, V loading (Mode I and II).

spring response corresponds well with the continuum solutions. This factor may only be applied for deep cracks ($a/t > 0.25$). It should be noted that correcting the yield surface yield stress with this factor results in a yield surface that should not be regarded as a true lower bound solution.

In load controlled structures, the reduced stiffness of the line spring results in predicting too large deformations, in displacement controlled structures this effect leads to prediction of somewhat too low load levels. Considering the loading in the hot spot region in a tubular joint, it behaves in displacement control for loads less than limit load. Hence should the model under investigation here be applicable for load versus displacement simulations.

Second, the line spring model provides a method for calculating J-integrals in a simplified way. Here, several inaccuracies may occur. As discussed in the model derivation section, there are possibilities in improving the constraint factor m calculation. The m_{II} factor should also be investigated further. For shallow cracks the relationship between crack tip opening displacement and ligament deformations have to be improved (Lee and Parks, 1993). The way the model is used in the present study, conservative crack tip opening displacements are obtained.

For the geometries investigated in the present study, in most cases the line spring based J was overpredicted in load control compared to the detailed FE results. In displacement control J was overpredicted somewhat, but in reasonable agreement with the continuum solutions. Inaccuracies in the elastic-plastic transition may be remedied by accounting for the crack tip plastic zone effect (Lee and Parks, 1995).

Due to the high ductility of the steels employed in the offshore industry, significant plasticity develops before any fracture initiation. Therefore, loss of a J-dominated stress and strain field due to loss of constraint in plastic crack tip deformations may develop. If this is true, then the basis for a J-based (one-parameter) fracture assessment disappears. Although a J-dominated crack tip region may exist in mixed mode (Aoki *et al.*, 1987), the computations of J herein are based on self-similar crack growth. This may not be representative for all materials, so there is a need for more research on mixed mode fracture characteristics in order to determine fracture mechanisms and valid fracture initiation parameters or damage evolution models. Ahmad *et al.* (1983) have obtained a correlation between the critical $\hat{J}_1$ component in mixed mode I/II and the Mode I critical J. If such criteria are valid, simple checks for crack criticality are possible.

The performance of the line spring model implemented in a shell FE program should be studied in the future. In this respect, the shell formulation should account for finite rotations (but small strains), as such deformations have significant effect on tubular joint load versus deformation behaviour (Skallerud, 1995).

REFERENCES

Ahmand, J., Barnes, C. R. and Kanninen, M. F. (1983). *An Elastoplastic Finite Element Investigation of Crack Initiation under Mixed Mode Static and Dynamic Loading.* ASTM STP 803 (eds C. F. Shih and J. P. Gudas), pp. I214–I239.

Aoki, S., Kishimoto, K., Yoshida, T. and Sakata, M. (1987). A finite element study of the near crack tip deformation fields of a ductile material under mixed mode loading. *J. Mech. Phys. Solids* **35,** 431–457.

Aoki, S., Kishimoto, K., Yoshida, T., Sakata, M. and Richard, H. A. (1990). Elastic-plastic fracture behaviour of aluminium under mixed mode loading. *J. Mech. Phys. Solids* **38,** 195–215.

Betegon, C. and Hancock, J. W. (1991). Two-parameter characterization of elastic-plastic crack-tip fields. *J. Appl. Mech.* **58,** 104–110.

Brocks, W., Kunecke, G., Noack, H. D. and Veith, H. (1989). On the transferability of fracture mechanics parameters from specimens to structures using FEM. *Nuclear Engng Design* **112,** 1–14.

Chao, Y. J., Yang, S. and Sutton, M. A. (1994). On the fracture of solids characterized by one or two parameters: theory and practice. *J. Mech. Phys. Solids* **42,** 629–647.

Cheaitani, M. J. and Burdekin, F. T. (1994). Ultimate strength of cracked tubular joints. In *Tubular Structures VI* (eds Grundy, Holgate and Wong), pp. 607–616.

Dodds, R. H. (1982). Effect of reduced integration on the 2-D quadratic isoparametric element in plane strain plasticity. *Int. J. Fract.* **19,** R75–R82.

Goldman, N. L. and Hutchinson, J. W. (1975). Fully plastic crack problems: the center cracked strip under plane strain. *Int. J. Solids Structures* **11,** 575–591.

Green, A. P. and Hundy, B. B. (1956). Initial plastic yielding in the notch bending test. *J. Mech. Phys. Solids* **4,** 128–144.

Gross, B. and Srawley, J. E. (1965). Stress intensity factors for single edged specimens in bending and combined bending and tension. NASA TD D-2603.
Hibbitt, Karlson, and Sorenson (1992). ABAQUS Manual, version 5.2.
Huang, X. and Hancock, J. W. (1988). The stress intensity factors of semi-elliptical cracks in a tubular welded T-joint under axial loading. *Engng Fract. Mech.* **30,** 25–55.
Hutchinson, J. (1968). Singular behaviour at the end of a tensile crack in a hardening material. *J. Mech. Phys. Solids* **16,** 13–31.
Ishikawa, H., Kitagawa, H. and Okamura, H. (1979). *J* integral of a mixed mode crack and its application. *Int. Conf. Mater.* **3,** 447–455.
Kishimoto, K., Aoki, S. and Sakata, M. (1980). On the path independent integral *J. Engng Fract. Mech.* **13,** 841–850.
Lee, H., and Parks, D. M. (1993). Fully plastic analyses of plane strain single edged cracked specimens subject to combined tension and bending. *Int. J. Fract.* **63,** 329–349.
Lee, H., and Parks, D. M. (1995). Enhanced elastic-plastic line spring finite element. *Int. J. Solids Structures* **32,** 2393–2418.
Li, F. Z., Shih, C. F. and Needleman, A. (1985). A comparison of methods for calculation of energy release rates. *Engng Fract. Mech.* **21,** 405–421.
McMeeking, R. M. and Parks, D. M. (1979). On criteria for *J*-dominance of crack tip fields in large scale yielding. ASTM STP 668 (eds Landes, Begley and Clarke), pp. 175–194.
Merkle, J. G. and Corten, H. T. (1974). A *J* integral analysis for the compact specimen, considering axial force as well as bending effects. *J. Press. Vessel Tech.* 286–292.
O'Dowd, N. P. and Shih, C. F. (1991). Family of crack-tip fields characterized by a triaxiality parameter—I. Structure of fields. *J. Mech. Phys Solids* **39,** 989–1016.
Parks, D. M. (1974). A stiffness derivative finite element technique for determination of crack tip stress intensity factors. *Int. J. Fract.* 487–502.
Parks, D. M. (1981). The inelastic line spring: estimates of elastic-plastic fracture mechanics parameters for surface cracked shells. *J. Press. Vessel Techn.* **103,** 246–254.
Parks, D. M. and White, C. S. (1982). Elastic-plastic line spring finite elements for surface cracked plates and shells. *J. Press. Vessels Tech.* **104,** 287–292.
Rice, J. (1968). A path independent integral and the approximate analysis of strain concentration by notches and cracks. *J. Applied Mech.* **35,** 379–386.
Rice, J. and Rosengren, G. F. (1968). Plane strain deformation near a crack tip in a power law hardening material. *J. Mech. Phys. Solids* **16,** 1–12.
Rice, J. and Levy, N. (1972). The part through surface crack in an elastic plate. *J. Applied Mech.* 185–194.
Rice, J. R. (1972). The line spring model for surface flaws. In *The Surface Crack Physical Problems and Computer Solutions* (ed. J. L. Swedlow), ASME.
Rice, J. R. (1975). Models for stable crack growth. In *Mechanics and Mechanisms of Crack Growth* (ed. M. J. May), British Steel Corp.
Shih, C. F. (1974). Small scale yielding analysis of mixed mode plane strain crack problems. In *Fracture Analysis*, ASTM STP 560, pp. 187–210.
Shih, C. F. and Hutchinson, J. W. (1976). Fully plastic solutions and large scale yielding estimates for plane stress crack problems. *J. Engng Mat. Tech.* **98,** 289–295.
Shih, C. F., German, M. D. and Kumar, V. (1981). An engineering approach for examining crack growth and stability. *Int. J. Press. Vessel Piping* **9,** 159–196.
Shih, C. F. and German, M. D. (1981). Requirements for a one-parameter characterization of crack tip fields by the HRR singularity. *Int. J. Fract.* **17,** 27–43.
Shih, C. F. (1981). Relationships between the *J*-integral and the crack opening displacement for stationary and opening cracks. *J. Mech. Phys. Solids* **29,** 305–326.
Shih, C. F. and Needleman, A. (1984). Fully plastic crack problems. Part 1: solutions by a penalty method. *J. Appl. Mech.* **51,** 48–56.
Shiratori, M. and Miyoshi, T. (1983). *Evaluation of J-Integral for Surface Cracks.* ASTM STP 803 (eds C. F. Shih and J. P. Gudas), pp. 1410–1424.
Skallerud, B., Eide, O. I. and Berge, S. (1994). Ultimate capacity of cracked tubular joints: comparison between numerical simulations and experiments. In *Proc. 7th Int. Conf. Behaviour of Offshore Structures* (*BOSS*), Vol. 3, pp. 241–259, Boston.
Skallerud, B. (1995). Inelastic line springs in nonlinear analysis of cracked tubular joints. *Fatigue Fract. Engng Mat. Struct.* **18,** 463–477.
Tada, Paris and Irwin (1973). *The Stress Analysis of Cracks Handbook*, Del Research Corp. Hellertown, PA, U.S.A.
White, C. S., Ritchie, R. O. and Parks, D. M. (1983). *Ductile Growth of Part-through Surface Cracks: Experiment and Analysis.* ASTM STP 803 (eds C. F. Shih and J. P. Gudas), pp. 1384–1409.